

# Tissue Discrimination through Force-Feedback from Impedance Spectroscopy in Robot-assisted Surgery<sup>\*</sup>

Brayden Kent, Angelica Cusipag, Carlos Rossa

Ontario Tech University, ON, Canada  
Faculty of Engineering and Applied Science  
brayden.kent@uoit.net  
angelica.cusipag@uoit.net  
carlos.rossa@uoit.ca

**Abstract.** Haptic force feedback in teleoperated robot-assisted minimally invasive surgery is difficult to implement with traditional force sensors at the tool tip. A novel approach to displaying forces to the user is explored using electric impedance spectroscopy with an electrode embedded needle. To give substance to the proposed method, user trials were conducted to compare the accuracy of inserting needles by hand and through electric impedance based haptic teleoperation. The results of the experiment suggest that, when compared to the control scenario, novice operators could accurately locate the phantom tumour with a high degree of accuracy and repeatability using force feedback derived from electric impedance spectroscopy.

**Keywords:** Robot-assisted Minimally Invasive Surgery · Electric Impedance Spectroscopy · Haptics

## 1 Introduction

Robot-assisted minimally invasive surgery (RMIS) has shown increasing promise in improving the quality of treatment in the operating room. Typically, the goal of teleoperated RMIS systems is to enhance the dexterity and precision of the surgeon rather than have robots replace them in the operating room. Through a remote console, the surgeon controls a robotic manipulator that operates on the patient. However, the lack of force feedback in the commercially available

---

\* We acknowledge the support of the Natural Sciences and Engineering Research Council of Canada (NSERC), the Canadian Institutes of Health Research (CIHR), and the Social Sciences and Humanities Research Council of Canada (SSHRC), [funding reference number NFRFE-2018-01986]. Cette recherche a été financée par le Conseil de recherches en sciences naturelles et en génie du Canada (CRSNG), par les Instituts de recherche en santé du Canada (IRSC), et par le Conseil de recherches en sciences humaines du Canada (CRSH), [numéro de référence NFRFE-2018-01986].

systems presents a steep learning curve for novice surgeons to become proficient in RMIS and achieve the desired levels of performance. In some minimally invasive procedures, the surgeon can rely on other forms of sensory feedback such as laparoscopic cameras to visualize the surgical site. Yet, this is not always a feasible solution for percutaneous procedures such as brachytherapy.

Alternatively, haptic feedback systems for RMIS can recreate the tool-tissue interaction contact force as a displayable force to the surgeon since it is an intuitive leap. In developing such haptic feedback, one tends to relate a physical property, such as tissue stiffness or contact force, to render the haptic force. Traditionally, there are two ways of developing the haptic force: measuring tool-tissue interaction forces directly or inferring them from measurements of the mechanical properties of the tissue. For needle based procedures, one can implement a force sensor at the base of the needle, outside of the body, to estimate the tissue composition during insertion. Unfortunately, friction along the needle shaft can obscure the data and consequently compromise the force feedback. To solve this, one can attempt to implement a force sensor at the tip of the needle. The challenge in integrating a force sensor at the tip is due to the constraints posed by the surgical environment, namely limited size and degrees of freedom [17].

However, tissues do need to be characterized solely on their mechanical properties, as organic tissues also have unique electric and dielectric properties. In the current state of the art, several instruments have been developed to differentiate healthy and cancerous cells through their electrical characteristics. NASA and BioLuminate Inc. developed a biopsy probe to identify breast cancer through electric impedance [1]. Yun et al. utilized an electrode embedded needle to identify thyroid cancer [21]. Park et al. integrated a microelectrode array onto a biopsy needle for liver cancer discrimination [19]. Measuring a tissue's response to electric stimulus at the tip of an electrode embedded needle can provide an alternative way to develop force feedback.

In this paper, an electrode embedded needle was developed to measure a tissue's electrical impedance through impedance spectroscopy, see Figure 1(c). As a robot manipulator inserts the needle into the tissue, the robot's operator can feel forces through a haptic device. Using a rudimentary model, the haptic force is developed from the tissue's electric impedance at the tip. The paper culminates with the proposed technique tested in user trials with gelatin phantoms to address its potential usability for future surgical procedures. The users were to find the gelatin layer that represented a cancerous tumour in two scenarios: inserting a needle by hand, and with an RMIS setup with haptic force feedback derived from the electric impedance model. While this paper has been written with a specific focus on differentiating cancer cells from healthy tissue in needle based RMIS, the proposed method could potentially be adapted to other tissue types and surgical procedures including fat in percutaneous liposuction, struvite crystals in nephrolithotomy and arterial plaque in angioplasty.

## 2 Electric Impedance Spectroscopy

The act of applying a spectrum of alternating current to an object to determine its composition is coined electric impedance spectroscopy (EIS) [2]. For decades, researchers have endeavoured to classify tissues based on their response to a spectrum of electric stimuli. Notably, as shown in [3], tissues exhibit unique and distinct electrical conductivities when exposed to various frequencies of alternating current. Halter *et. al* have shown that in a prostate; glandular tissue, stroma, carcinoma and benign hyperplasia have distinct ranges of conductivity and relative permittivity [7]. Furthermore, cancerous breast tissue have significantly different impedivity modulus and phase angle than healthy breast tissues [8]. Typically, the instruments used in EIS resemble one of the configurations shown in Figure 1. With a current source based device, it is possible to limit the amount of current seen by the tissue, making it a safer choice for biomedical applications.

Classification of electric parameters for biological tissue is a vast and challenging field of research. Over the past few decades, researchers have been exploring new models for bioimpedance measurements. For the extent of this paper it is sufficient to recognize the following: The first, that a given tissue has a frequency dependent electric impedance and can be determined using EIS. Secondly, that two different tissues can be discriminated by their respective regions of electric impedance.

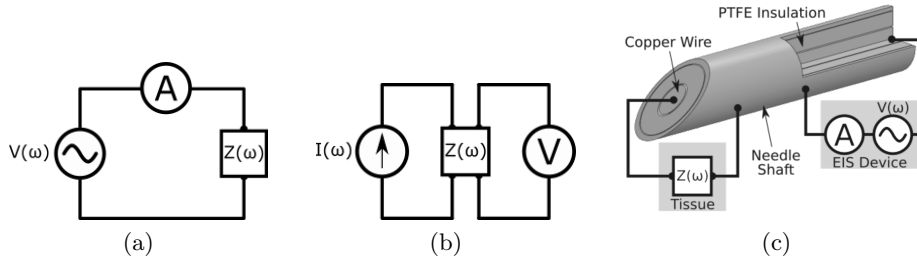


Fig. 1: A simplified bipolar spectroscopy measurement (a): two electrodes are attached to an object with unknown, frequency dependent impedance  $Z(\omega)$  where a voltage is applied and current is measured in line. A simplified tetrapolar spectroscopy measurement (b): the applied signal electrodes are separate from the measurement electrodes, requiring four electrodes attached to the object. (c) An example of a bipolar electrode arrangement with an electrode embedded needle.

In traditional circuit analysis, one can determine the resistance of a circuit element through Ohm's Law by applying an electric signal (voltage or current) and measuring the corresponding property (current or voltage). If an alternating current with frequency  $\omega$  is applied, the impedance  $Z(\omega)$  of the element, a combination of resistance  $R$  and reactance  $X(\omega)$ , can be evaluated as

$$Z(\omega) = R + jX(\omega) \quad (1)$$

It is well recognized that tissues exhibit behaviour of resistance and capacitive elements. To truly capture the behaviour, one must look at the electrochemical behaviours of the cells that comprise the tissue. In gist, cell structures react to an electric field through polar molecule alignment and relaxation. This behaviour is encompassed in a popular electrochemical model proposed by Debye and adapted by Cole [4] [15],

$$Z(\omega) = \frac{R + (R_o - R_\infty)}{1 + (j\omega/\omega_o)^\alpha} \quad (2)$$

where  $R_o$  and  $R_\infty$  correspond to the low and high frequency intercepts of the complex impedance plane, see Figure 2(a), respectively.  $\omega_o$  represents “turnover” frequency [15]. The constant  $0 < \alpha \leq 1$  defines the angle between the complex impedance locus arc and the intercepts [15]. The model in (2) can be fitted to an equivalent circuit of which is comprised of two resistors and a constant phase element (CPE), see Figure 2(b).

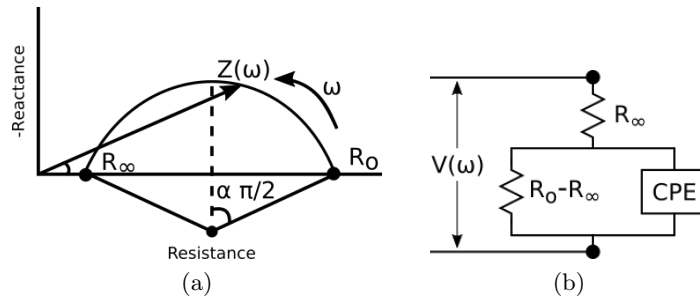


Fig. 2: (a) A typical Cole-Cole plot in the complex impedance plane that represents how a biological tissues electric impedance can change with an applied alternating current of frequency  $\omega$ . (b) An equivalent circuit model for biological tissue with Cole parameters [4] [15].

Provided that one can now differentiate two tissues given their electric impedance the following section derives how this property can be used in haptic force feedback.

### 3 Developing Force Feedback

Alas, there is no known direct correlation between the electrical and mechanical properties for organic tissue. When comparing malignant to healthy cells in glandular organs, such as breast or prostate, malignant cells are generally more stiff and have greater electric impedance [6] [13] [8] [10]. However, cancerous cells can offer better electrical conductivity relative to healthy tissue, as seen in liver cancer [11]. Thus, the model proposed here should be adapted accordingly

depending on the application. A crude model can be made, where the mechanical stiffness  $K$  is proportional to the electrical impedance  $Z(\omega)$  of a given tissue,

$$K = \gamma_1 Z(\omega) \quad (3)$$

where  $\gamma_1$  is a conversion factor. The conversion factor will differ for any given tissue and should be calibrated for the specific situation.

It has been shown elsewhere that for needle-tissue interaction that the force at the base of the needle is comprised of three parts: puncturing, cutting and friction. [9] [20] To simplify the model, assume that the needle has already punctured the tissue. Furthermore, eliminating the friction component will improve the haptic feedback for tissue discrimination. Thus, only cutting forces are presented where the force at the base of the needle  $F$  is proportional to the tissue stiffness  $K$  through a factor  $\gamma_2$ ,

$$F = \gamma_2 K \quad (4)$$

In combining (3) and (4) a lumped conversion factor  $\gamma = \gamma_1 \gamma_2$  relates electric impedance to force,

$$F = \gamma Z(\omega) \quad (5)$$

Consider a needle with EIS electrodes at the tip that has punctured an organ which is comprised of healthy cells with a tumor at an unknown depth. The electric impedance of the tissue at the tip can be evaluated by averaging  $n$  electric impedance measurements. To discriminate between the two tissues, the electric impedance data is compensated to be relative to the measurement immediately after puncturing the tissue. The initial electric impedance  $Z(\omega, 0)$  is consequently removed from measurements at needle tip depth  $d$ . The haptic force can then be estimated as,

$$F(d) = \gamma \left( \frac{\sum_{i=1}^n Z_i(\omega, d)}{n} - Z(\omega, 0) \right) \quad (6)$$

In summary, using EIS, one can determine the local electric impedance at the tip of the needle and render that as a force  $F$  to the user. The haptic force can be adjusted through a tunable parameter  $\gamma$ .

With the relationship between the electric impedance and haptic force now developed, the following section describes the RMIS setup and phantom tissues used to test the proposed force feedback model.

## 4 Experimental Setup

The experimental setup used to validate the concept is shown in Figure 3.

The Meca500 6-DOF serial robot arm (Mecademic, Québec, Canada) inserts an electrode embedded needle as controlled by the operator with the Novint Falcon 3-DOF parallel manipulator haptic joystick (Novint Technologies, New Mexico, USA). The impedance data gathered by a spectroscopy system is then

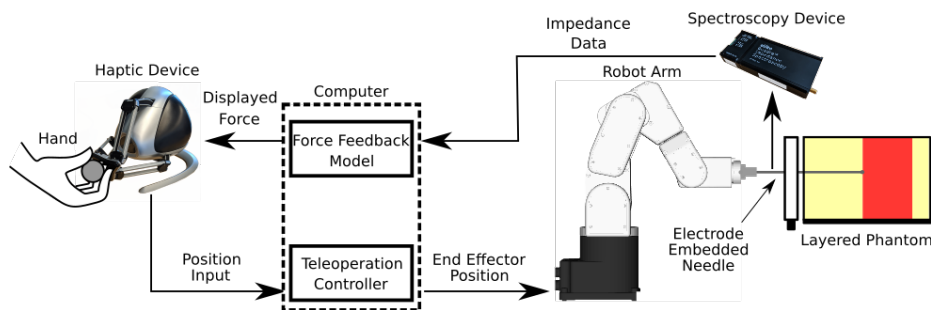
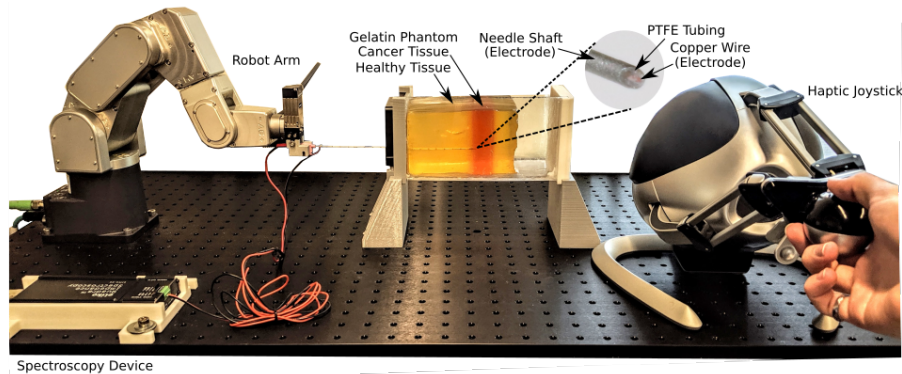


Fig. 3: The experimental setup: the haptic device controls the needle insertion depth as the robotic arm inserts the needle into the phantom tissue. The electrode at the tip of the needle is used by the spectroscopy device to determine the local electric impedance of the phantom. The impedance is converted to a force and displayed to the user as haptic feedback.

used in the force feedback model to display a force to the user through the haptic device.

The electrode embedded needle was fabricated following the design shown in Figure 1(c), see Figure 3. An 18 gauge brachytherapy needle (Eckert & Ziegler, New York, USA) was modified for the experiment. Enamelled copper wire was fed through the shaft and served as the primary electrode. The needle shaft itself acted as the secondary electrode. A PTFE sleeve was used as an additional means of insulation between the primary and secondary electrode. Cyanoacrylate was used to bond the assembly. Fine grit sandpaper was used to strip the enamel of the copper wire and expose the tip of the electrode. While the developed electrode embedded needle is primitive and impedes its ability to deposit radiation for brachytherapy, further refinement of the design can be done to miniaturize the electrodes as seen in [19].

Using the electrode embedded needle the Quadra electric impedance spectroscopy device (Eliko, Tallin, Estonia) [16] was used to measure the electric impedance of a phantom tissue. The analogue front end of the module was con-

nected to the electrode embedded needle to form a bipolar EIS measurement scheme.

#### 4.1 Phantom Tissue Properties

The phantom tissue was made using unflavoured porcine gelatin. Three layers of gelatin were created to fabricate one of the phantoms used in testing: a cancer layer adjacent to healthy tissue on either side, refer to Figure 3. For the healthy tissue, a ratio of 25 grams of gelatin with 5 grams of iodized salt was added to 240 millilitres of water. To make the cancerous layer, the ratio used was 40 grams of gelatin to 240 millilitres of water.

The healthy and cancerous phantom types were prepared such that they would acquire unique mechanical and electrical properties. The stiffness of the gelatin phantoms was measured through indentation tests. The tests were repeated at set internal temperatures, as the mechanical properties of the gelatin were temperature dependent. The Young's modulus  $K$  was determined with the relation [18] [12],

$$K = \frac{(1 - v^2)F_k}{2ax\kappa} \quad (7)$$

where  $x$  and  $F_k$  are the indentation depth and force, respectively,  $a$  is the radius of the cylinder indenter, and  $\kappa$  was taken as unity since the indenter radius was significantly smaller than the surface area of the phantom. Poisson's ratio  $v$  was approximated as 0.45, a value between the those seen in the literature, 0.4 [14] and 0.495 [5].

The Young's modulus of the phantom was determined using data from four different internal temperatures with five compressions each. The Young's modulus for the healthy tissue gelatin phantom and the cancerous gelatin phantom were determined to be  $6.88 \pm 0.10$  kPa and  $12.0 \pm 0.17$  kPa respectively at 14°C. These values are comparable to those obtained for gelatin phantoms in other publications [5]. The created phantoms are less stiff than actual human organs but do mirror the behaviour of prostate cancer, which has nearly twice the elastic modulus of healthy tissue [10].

## 5 Experiment Results

The model formulated in (6) is integrated in the system shown in Figure 3. The complete results of the experiment are in shown in Figure 4.

An unmodified 18 gauge brachytherapy needle was attached to a load cell to determine the axial insertion force, see Figure 4 (b). This plot is representative of the force the surgeon would feel by inserting the needle by hand. The three components of the needle-tissue interaction are clearly visible: cutting, friction and puncturing. Noticeably, the slope of the force increases while transitioning into the cancer phantom. This is a result of the increased stiffness created by altering the water to gelatin ratio in the phantom fabrication for the respective

layers. The overall difference in force seen along the needle depth is relatively inappreciable, which would make it difficult to distinguish between the tissue types while inserting by hand. Thus, for the haptic feedback RMIS scenario, it is prudent that the force be more discernible for the transition into the cancer layer.

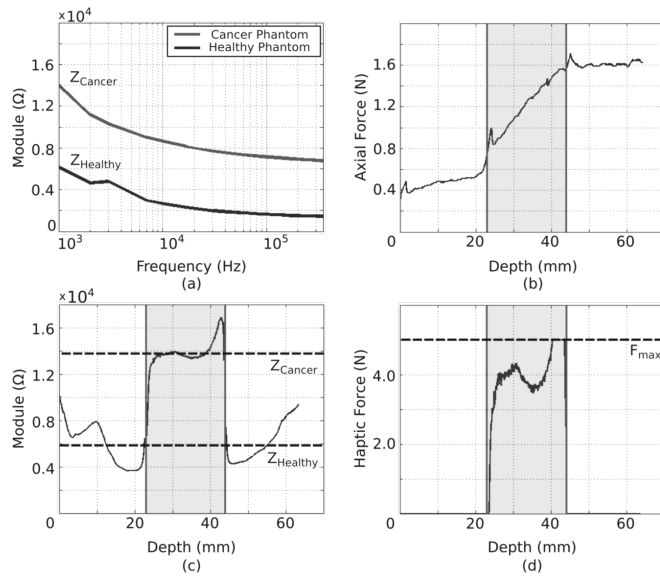


Fig. 4: Experimental results: differentiating the phantom layers.

Figure 4(a) showcases the difference in electric impedance of the gelatin layers with respect to an alternating frequency  $\omega$  through EIS measurements. The addition of salt in the healthy gelatin resulted in a distinctly different conductivity compared to the cancerous layer. The impedance data shown in Figure 4(a) is not compensated for the impedance of the electrode embedded needle. It is reasonable to expect that the needle would introduce both resistance and capacitance and consequently have an impact on the measured values. However, in this application we are not attempting to classify the composition of the phantom, rather, the application is to distinguish between the layers that compose it. Since the properties of the needle do not change through the insertion, its effect is considered negligible.

In the RMIS control loop the magnitude of the phantom's electric impedance at the needle tip was determined by averaging  $n = 10$  spectra samples. The electric impedance at lower frequencies provided the greatest relative difference in the tissue types as shown in Figure 4(a), thus the electric impedance at  $\omega = 1$  kHz was used in calculating the displayed force in (6).

The electrode embedded needle was inserted into the tissue and the impedance at a given depth was recorded, see Figure 4(c). These impedance values are evaluated as a force to be displayed to the user as shown in Figure 4(d). For any  $F(d) < 0$  was taken as  $F(d) = 0$ , otherwise the haptic device would pull the user in rather than impede their insertion. Furthermore, to provide a safe limit to the displayable force any  $F(d) > F_{max}$  was set such that  $F(d) = F_{max}$ . In comparison to (b), the force is significantly more noticeable during the transition into the cancer phantom.

The results of the experiment suggested that the haptic feedback would be more detectable than inserting the needle manually.

## 6 User Trial Study

An additional study was conducted to test if the method was applicable to a more pragmatic scenario. A set of user trials were designed to mimic a surgeon inserting a needle during percutaneous brachytherapy. First, the user would insert the needle by hand into unique phantoms, see Figure 5(a). Second, the user would control the robot arm through the haptic device, where they would detect the force based on EIS, see Figure 5(b). The participant's objective was to determine where the cancer layer existed in the gelatin phantom using only force feedback. In the hand trial the user would stop inserting the needle when they perceived the cancer layer, and leave it within the tissue. In the teleoperated test, the user would press a button on the haptic device handle to signal the change in tissue and record the needle tip depth.

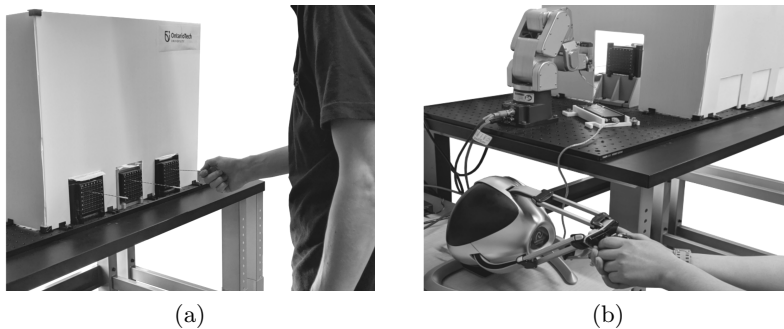


Fig. 5: The two stages of the user trials. (a) The test participant would first insert the needle by hand to determine the depth of the cancer layer in three unique phantoms. (b) The participant would then determine the depths using haptic feedback in the teleoperated scenario.

Three different phantoms were used, with the cancer layer at different depths. The test participant was unable to view any of the phantoms, similar to a black

box problem. The participant would insert the electrode embedded needle into the phantom through a grid template.

The user trials consisted of  $N = 16$  participants. All participants were given the same set of written instructions prior to the start of the test. Each participant was shown an example gelatin phantom that they could practice with hand insertion to familiarize themselves with the needle force associated with the healthy and cancerous layers of the gelatin. Additionally, a simulated force was presented to the user in the haptic device such that they could recognize the haptic force they were to expect in the actual trials. Each participant was only permitted to one insertion per phantom.

### 6.1 User Study Test Results

Figure 6 shows the final depths that the user perceived the cancer for both tests in each of the three phantoms.

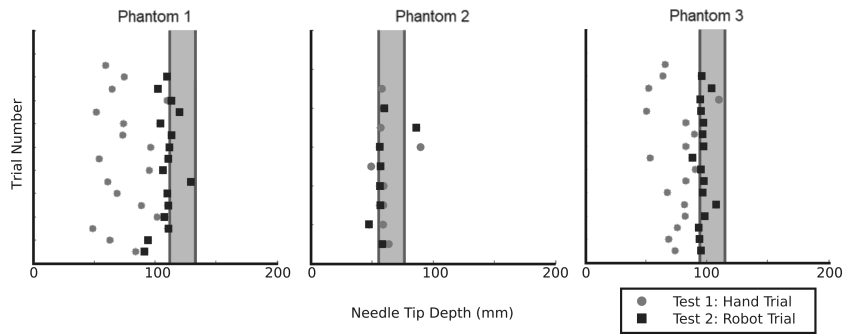


Fig. 6: Results of the user trials in each of the three phantoms. The shaded region represents the cancer layer of the phantom.

Noticeably, the teleoperated trials performed significantly better than the hand trials overall. The hand trials were more successful at finding the cancer layer in Phantom 2, where the layer was at a shallow depth. It is speculated that the users had more difficulty in Phantom 1 and Phantom 3 hand trials due to the amount of friction experienced. In the teleoperation scenario, friction is eliminated, since the haptic device only displayed a force from the electric properties of the phantom, which may explain the increase in performance.

Many of the teleoperated results show final depths recorded before the transition line. This is a result of two circumstances. First, while the gelatin layers were prepared separately, when combined in the phantom, the salt ions diffuse gradually into the non-salinated layer which alters the local conductivity near the layer transition. Second, the haptic force pushes against the user, causing them to unintentionally move the joystick handle slightly outward and consequently move the needle out of the cancer. For the latter it can be seen in the

Phantom 2 and Phantom 3 results that the users more readily anticipate the haptic force and become more consistent in stopping within the cancer layer.

Table 1: User Trial Statistics (Units are in [mm])

	<b>Phantom 1</b>		<b>Phantom 2</b>		<b>Phantom 3</b>	
	Cancer Start:	112.5	Cancer Start:	56.0	Cancer Start:	94.5
	Cancer End:	134.5	Cancer End:	78.0	Cancer End:	116.5
	<b>Avg Depth</b>	<b>Success</b>	<b>Avg Depth</b>	<b>Success</b>	<b>Avg Depth</b>	<b>Success</b>
Test 1: Hand	74.9 ± 18.5	0%	61.7 ± 11.1	78%	72.5 ± 15.5	6%
Test 2: Robot	109.1 ± 9.1	25%	59.9 ± 11.3	75%	96.6 ± 4.3	81%

The average depth with standard deviation for each of the phantoms in the two test scenarios are listed in Table 1 along with the percentage of trials that successfully finished within the cancer layer.

## 7 Conclusion

Implementing traditional force sensors on needles for haptic feedback in teleoperated RMIS is not a trivial task. This paper introduces an alternative through analysis of a tissue’s electric impedance. Electric impedance spectroscopy was performed with an electrode embedded needle in gelatin phantoms. The method was tested with user trials and compared to a control scenario to evaluate its effectiveness.

The user trials and experimental results indicate that the addition of haptic feedback derived from the spectroscopy data improved the operators ability to detect where the cancer layer started in the phantom tissue. The proposed method of using electric impedance to display haptic feedback may hold new possibilities in several medical procedures including percutaneous brachytherapy, nephrolithotomy and angioplasty. At a minimum, it is worthwhile to further explore and develop this new avenue of providing haptic feedback as a substitute or supplement to conventional methods of sensory feedback.

## References

1. Andrews, R.J., Mah, R.W.: The NASA smart probe project for real-time multiple microsensor tissue recognition. *Stereotactic and functional neurosurgery* **80**(1-4), 114–119 (2003)
2. Barsoukov, E., Macdonald, J.R.: *Impedance spectroscopy: theory, experiment, and applications*. John Wiley & Sons (2018)
3. Brown, B.H.: Electrical impedance tomography (EIT): a review. *Journal of medical engineering & technology* **27**(3), 97–108 (2003)

4. Cole, K.: Dispersion and absorption in dielectrics. *J. Chem. Phys* **9**, 341 (1941)
5. Hall, T.J., Bilgen, M., Insana, M.F., Krouskop, T.A.: Phantom materials for elastography. *IEEE transactions on ultrasonics, ferroelectrics, and frequency control* **44**(6), 1355–1365 (1997)
6. Halter, R.J., Schned, A., Heaney, J., Hartov, A., Paulsen, K.D.: Electrical properties of prostatic tissues: I. single frequency admittivity properties. *the Journal of Urology* **182**(4), 1600–1607 (2009)
7. Halter, R.J., Schned, A., Heaney, J., Hartov, A., Schutz, S., Paulsen, K.D.: Electrical impedance spectroscopy of benign and malignant prostatic tissues. *The Journal of urology* **179**(4), 1580–1586 (2008)
8. Jossinet, J.: The impedivity of freshly excised human breast tissue. *Physiological measurement* **19**(1), 61 (1998)
9. Khadem, M., Rossa, C., Usmani, N., Sloboda, R.S., Tavakoli, M.: A two-body rigid/flexible model of needle steering dynamics in soft tissue. *IEEE/ASME Transactions on Mechatronics* **21**(5), 2352–2364 (2016)
10. Krouskop, T., Wheeler, T., Kallel, F., Garra, B., Hall, T.: Elastic moduli of breast and prostate tissues under compression. *Ultrasonic imaging* **20**(4), 260–274 (1998)
11. Laufer, S., Ivorra, A., Reuter, V.E., Rubinsky, B., Solomon, S.B.: Electrical impedance characterization of normal and cancerous human hepatic tissue. *Physiological measurement* **31**(7), 995 (2010)
12. Lehmann, T., Rossa, C., Usmani, N., Sloboda, R.S., Tavakoli, M.: Intraoperative tissue young's modulus identification during needle insertion using a laterally actuated needle. *IEEE Transactions on Instrumentation and Measurement* **67**(2), 371–381 (2017)
13. Li, Q., Lee, G.Y., Ong, C.N., Lim, C.T.: AFM indentation study of breast cancer cells. *Biochemical and biophysical research communications* **374**(4), 609–613 (2008)
14. Markidou, A., Shih, W.Y., Shih, W.H.: Soft-materials elastic and shear moduli measurement using piezoelectric cantilevers. *Review of Scientific Instruments* **76**(6), 064302 (2005)
15. McAdams, E., Jossinet, J.: Tissue impedance: a historical overview. *Physiological measurement* **16**(3A), A1 (1995)
16. Min, M., Lehti-Polojärvi, M., Hyttinen, J., Rist, M., Land, R., Annus, P.: Bioimpedance spectro-tomography system using binary multifrequency excitation. *International Journal of Bioelectromagnetism* **209**, 76–79 (05 2018). <https://doi.org/10.18154/RWTH-CONV-224930>
17. Okamura, A.M.: Haptic feedback in robot-assisted minimally invasive surgery. *Current opinion in urology* **19**(1), 102 (2009)
18. Ottensmeyer, M.P., Salisbury, J.K.: In vivo data acquisition instrument for solid organ mechanical property measurement. In: *Int. Conf. on Medical Image Computing and Computer-Assisted Intervention*. pp. 975–982. Springer (2001)
19. Park, J., Choi, W.M., Kim, K., Jeong, W.I., Seo, J.B., Park, I.: Biopsy needle integrated with electrical impedance sensing microelectrode array towards real-time needle guidance and tissue discrimination. *Scientific reports* **8**(1), 264 (2018)
20. Rossa, C., Tavakoli, M.: Issues in closed-loop needle steering. *Control Engineering Practice* **62**, 55–69 (2017). <https://doi.org/10.1016/j.conengprac.2017.03.004>
21. Yun, J., Hong, Y.T., Hong, K.H., Lee, J.H.: Ex vivo identification of thyroid cancer tissue using electrical impedance spectroscopy on a needle. *Sensors and Actuators B: Chemical* **261**, 537–544 (2018)